RESEARCH ARTICLE

Macromolecular Rapid Communications
www.mrc-journal.de

Mesoporous Organic/Inorganic Hybrid Materials with Frank-Kasper Phases Templated by an Unusual Linear Symmetry Diblock Copolymer

*Wei-Cheng Chen, Yuan-Tzu Liu, and Shiao-Wei Kuo**

In this study the authors used an unusual linear symmetric poly(ethylene oxide-b-caprolactone) (PEO-b-PCL) diblock copolymer as a template within phenolic/double-decker silsesquioxane (DDSQ) hybrids to synthesize mesoporous phenolic/DDSQ materials having Frank–Kasper (FK) phases (e.g., σ, A15, H, and Z phases). These FK structures are the first to have been prepared using a block copolymer and the first to exist in mesoporous materials. The authors' mesoporous carbon/DDSQ hybrids displayed high capacitance (764 F g^{-1} at a current of 0.5 A g^{-1} and 98.4% capacitance retention over 2000 cycles), arising from their high surface areas, high pore volumes, and tunable concentrations of N, O, and Si heteroatoms.

1. Introduction

Frank–Kasper (FK) phases with highly ordered local and complex lattices were first observed in metal alloys; they feature topologically close-packed polyhedra having a coordination number (CN) of 12, 14, 15, or 16, with at least one polyhedron having a CN of greater than 12. These tetrahedra are not all exactly highly regular because the partition of space with only regular tetrahedra is not possible; thus, they become slightly distorted.[1] At present, 28 different types of FK phases have been observed experimentally; several, including the A15, σ, H, Z, C14, and C15 phases, have also been found in the self-assembled structures of soft-matter systems, including low-molecular-weight surfactants, liquid crystals, block copolymers, dendrimers, and giant amphiphiles.[2]

Similar to the metal alloys that use atoms as their motifs, the organic or hybrid materials that form FK phases initially self-assemble into spheroidal micelles that then organize into supramolecular lattices.[3] For example, the microphase separation of diblock copolymers can induce self-assembled structures—including lamellae (LAM), bicontinuous double gyroids (DG), hexagonally packed cylinders (HPC), and body-centered cubic (BCC) structures—with a symmetrical phase diagram, the result of the distinct characteristics of the two polymer segments connected through a covalent bond.[4] For many years, only the BCC structure was predicted and found in compositionally asymmetric diblock copolymers, although FK A15 and σ phases have also been observed in some block conformations or architectures of asymmetry.[3] Chanpuriya et al. found that a complex tetrablock copolymer (ABAC) sequence could form an A15 phase in a small window of composition at certain temperatures while heating; thus, nonlinear architectures (e.g., ABCA or AB_n "miktoarm" stars) were generally believed to be the only approaches toward FK phases.[5] Nonetheless, architectural or conformational asymmetry in even simple linear diblock copolymers having different statistical block segment lengths has also been implicated recently to form A15 or σ phases.[6] Bates et al. reported that a simple poly(dodecyl acrylate-*b*-lactide) (PDDA-*b*-PLA) diblock copolymer having a minority LA volume fraction ($f_L = 0.25$–0.33) could form the A15 sphere phase, based on small-angle X-ray scattering (SAXS) experiments and self-consistent field theory (SCFT) calculations.[7] Nevertheless, the formation of such unconventional FK phases from simple linear diblock copolymers remains challenging because it can be difficult to synthesize them with controllable volume fractions through living polymerizations.[8]

A simpler approach toward controlling the volume fraction is to blend a diblock copolymer with a homopolymer. For example, Mueller et al. reported that the blending of poly(styrene-*b*-1,4-butadiene) with poly(1,4-butadiene) (PS-*b*-PB/PB, classified as A-*b*-B/B) led to the formation of FK σ, C14, and C15 phases.[9] The pure PS-*b*-PB diblock copolymer having a minor fraction of PB ($f_B = 0.18$) with conformational and compositional asymmetry formed the BCC structure, as expected. Remarkably, however, when blending with the PB homopolymer at a molecular weight ($M_{B,homo}$) similar to that of the PB block ($M_{B,block}$) in the diblock copolymer ($\alpha = M_{B,homo}/M_{B,block} = 1.08$), these PS-*b*-PB/PB blends formed FK σ, C14, and C15 phases upon increasing the PB concentrations. In contrast, blending with a lower molecular weight of PB ($\alpha = 0.6$) led only to BCC and HPC structures upon increasing the PB concentrations. This phase behavior can

Dr. W.-C. Chen, Y.-T. Liu, Prof. S.-W. Kuo
Department of Materials and Optoelectronic Science
National Sun Yat-Sen University
Kaohsiung 80424, Taiwan
E-mail: kuosw@faculty.nsysu.edu.tw
Prof. S.-W. Kuo
Department of Medicinal and Applied Chemistry
Kaohsiung Medical University
Kaohsiung 807, Taiwan

The ORCID identification number(s) for the author(s) of this article can be found under https://doi.org/10.1002/marc.202100302

DOI: 10.1002/marc.202100302

be rationalized in terms of "dry" and "wet" brush behavior in the diblock copolymer/homopolymer blends. The higher molecular weight of PB led to stronger localization in the spherical phase, swelling the spheres to form diblock cores and, thereby, inducing FK phases to fill the space, because of the optimal minimal surface solution and maximizing the local particle sphericity; this behavior was also predicted using self-consistent field theory (SCFT) in dry-brush mode.[9] The "wet" brush behavior of the diblock copolymer/homopolymer blend has been observed when blending not only a lower molecular weight of the homopolymer ($\alpha < 1$) but also a higher molecular weight of the homopolymer (even $\alpha > 1$) if the diblock copolymer/homopolymer blend (usually classified as A-*b*-B/C) featured strong hydrogen bonding between the B and C block segments.[10] For example, we have observed that poly(styrene-*b*-vinylphenol)/poly(4-vinylpyridine) diblock copolymer/homopolymer blends exhibit wet-brush behavior, transitioning from LAM to DG to HPC to BCC structures, upon increasing concentration of the poly(4-vinylpyridine) homopolymer.[11] The question remained whether we could simply blend a linear symmetric diblock copolymer (LAM phase) with a homopolymer, copolymer, or organic/inorganic hybrid to form FK phases by varying the volume fraction of the diblock copolymer segment.

Exploiting hydrogen bonding in diblock copolymer/homopolymer blends to prepare mesoporous materials (e.g., phenolic, carbon, silica, and phenolic/silica and carbon/silica hybrids) with pore sizes in the range from 2 to 50 nm has been investigated widely during the last 20 years because this approach provides high chemical functionality, tunable macroscopic forms, and various mesopore structures (e.g., HPC, DG, and BCC phases).[12] Using the low-molecular-weight surfactants *N*-myristoyl-L-glutamic acid and hexadecyltrimethylammonium bromide (CTAB) as templates has resulted in the formation of mesoporous silicas displaying dodecagonal tiling patterns, including FK σ, A15, and H phases.[13] Nevertheless, a low molecular weight surfactant (e.g., CTAB) is limited in its ability to tune the pore size (<4 nm); accordingly, poly(ethylene oxide)-based diblock copolymers (e.g., poly(ethylene oxide-*b*-styrene) [PEO-*b*-PS], poly(ethylene oxide-*b*-caprolactone) [PEO-*b*-PCL]) have been employed to provide mesoporous materials (pore sizes: 5–50 nm) having larger pores and long range order.[14] Nevertheless, mesoporous materials with FK phases templated by linear symmetric diblock copolymers have not been reported previously, to the best of our knowledge. Herein, we demonstrate that mesoporous phenolic/DDSQ and carbon/DDSQ materials having FK phases (namely σ, A15, H, and Z phases) can be prepared when using a linear symmetric PEO-*b*-PCL diblock copolymer as the template; these FK phases are the first to have been prepared using a linear symmetric block copolymer and the first to have been observed in a mesoporous materi

2. Results and Discussion

Over the last decade, our group has widely investigated the blending of the linear symmetric diblock copolymer PEO_{114}-*b*-PCL_{87} ($f_{PCL} = 0.67$, LAM) with phenolic resin, tetraethyl orthosilicate (TEOS), and phenolic/TEOS mixtures to prepare mesoporous phenolics, silicas, and phenolic/silica hybrids, but we have observed only typical mesoporous structures (e.g., DG, HPC, and BCC structures).[14b,15] Cheng et al. found that various hybrid macromolecules derived from polyhedral oligomeric silsesquioxane (POSS) displayed various FK phases (σ, A15, and Z phases)—namely, i) amphiphilic giant tetrahedron POSS cages (one hydrophilic and three hydrophobic POSS cages);[16] ii) POSS-based giant surfactants, one hydrophilic POSS cage (DPOSS) and different molecular topologies of hydrophobic PS with various tails (DPOSS-*N*PS_m), where is N is the number of tails and m is molecular weight of each PS tail; iii) six POSS cages on the triphenylene core; and iv) AB_n dendron-like giant molecules of DPOSS-M$POSS_n$, where n is number of hydrophobic POSS cages (MPOSS).[17] Inspired by those results, we suspected that a matrix of POSS cages in phenolic resin, templated by a linear symmetric diblock copolymer, might provide various FK phases. The architectures of polymer/POSS hybrids are, however, strongly dependent on the functionality of the POSS derivative (e.g., mono, multi-, and bifunctionalized POSS cages).[18] Only a bifunctionalized POSS, prepared using double-decker silsesquioxane (DDSQ), can form main chain-type POSS units and, thus, be soluble in various organic solvents and allow the preparation of mesoporous materials; in contrast, even a low concentration of multi-functional POSS units in a phenolic resin results in insoluble cross-linked phenolic/POSS hybrids.[19] In a previous study, we reacted a bifunctionalized phenolic DDSQ, phenol, and CH_2O in the presence of NaOH to incorporate various amounts of DDSQ into phenolic/DDSQ (PDDSQ) hybrids (**Scheme 1**a; Table S1, Supporting Information).[20]

We obtained mesoporous PDDSQ hybrids after templating with a PEO-*b*-PCL (EC) diblock copolymer, thermally curing at 150 °C for 24 h (Scheme 1b) to form self-assembled structures, and then pyrolyzing them at 400 °C for 6 h (Scheme 1c).

Figure S1, Supporting Information, presents SAXS patterns of the PDDSQ-30/EC = 70/30 hybrid before and after thermal calcination. Prior to thermal calcination, the pattern of the PDDSQ-30/EC = 70/30 hybrid displayed a broad peak at a value of q of 0.147 nm^{-1} (d = 42.72 nm), indicating a mesostructure of short-range order; in contrast, the long-range order of an HPC mesostructure (with peak ratios of $1:\sqrt{3}:\sqrt{4}:\sqrt{7}:\sqrt{9}:\sqrt{12}$) appeared after thermal calcination, with the first scattering peak shifted to 0.211 nm^{-1} (d = 29.76 nm). The highly ordered scattering peaks became sharp and the d-spacing decreased because removal of the EC template led to pore formation, a greater contrast in electron density, and shrinkage of the mesoporous PDDSQ hybrid matrix.[15] **Figure 1** displays the SAXS patterns, TEM images, and N_2 sorption isotherms of the mesoporous PDDSQ hybrids prepared from various PDDSQ-30/EC mixtures. The SAXS patterns of the mesoporous PDDSQ hybrids obtained from the PDDSQ-30/EC = 50/50 (Figure 1a), 60/40 (Figure 1b), and 70/30 (Figure 1c) mixtures all displayed the long-range order of HPC mesostructures (with peak ratios of $1:\sqrt{3}:\sqrt{4}:\sqrt{7}:\sqrt{9}:\sqrt{12}$) after thermal calcination, as confirmed using TEM (Figure 1e,f); the d-spacing decreased from 31.55 to 29.76 nm upon increasing the concentration of PDDSQ. Figure 1i–k presents the corresponding N_2 sorption isotherms; we observed typical type-IV curves with H_1-like hysteresis appearing at relative pressures from 0.80 to 0.95, implying a common type of mesoporous structure with well-defined cylindrical pore channels and a narrow pore size distribution from 9.4 to 14.1 nm. Most importantly, the mesoporous PDDSQ hybrid prepared from the

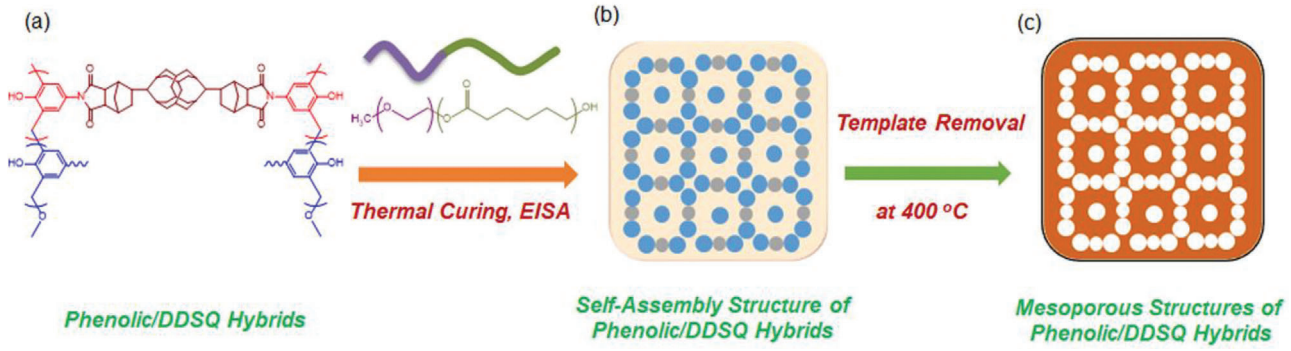

Scheme 1. Preparation of c) mesoporous structures of phenolic/DDSQ hybrids from a) phenolic/DDSQ (PDDSQ) hybrids and b) self-assembled structure of phenolic/DDSQ hybrids after removal of the PEO-*b*-PCL template at 400 °C.

PDDSQ-30/EC = 80/20 mixture (Figure 1d) provided a SAXS peak ratio of $\sqrt{2}:\sqrt{4}:\sqrt{5}:\sqrt{6}:\sqrt{14}:\sqrt{16}$, corresponding to the A15 phase, as revealed by TEM (Figure 1h). The SAXS pattern suggested a cube unit cell having a value of a of 67.73 nm; the TEM image in Figure 1h displayed the real space of a sphere arrangement along the [001] direction of the A15 phase, with the distance between two neighboring squares giving a value of a of 60.46 ± 4.03 nm, close to that measured from the SAXS data. The spheres in the green-dashed circles in Figure S2a, Supporting Information, correspond to the gray spheres in Figure S2b, Supporting Information, with a CN of 12 (pore size = 8.33 ± 0.63 nm).[16] These spheres are smaller than their neighbors with a CN of 14 (blue spheres in Figure S2b, Supporting Information; pore size = 12.67 ± 1.15 nm). The average size ratio between these two types of spheres was 1.52 ± 0.05, calculated based on the TEM image (Figure 1h or Figure S2a, Supporting Information). Unlike other A15 phases of soft-matter systems (e.g., surfactants, block copolymers, dendrimers, and giant amphiphiles),[2] the N_2 sorption isotherms of our mesoporous A15 phase could provide the pore size distribution (Figure 1l). We observed two sizes of mesopores, based on the Harkins and Jura model: the mean pore sizes from the adsorption branch were 8.6 nm, corresponding to the gray spheres in Figure S2b, Supporting Information, having a CN of 12 and 12.5 nm, due to the blue spheres in Figure S2b, Supporting Information, having a CN of 14. The average size ratio of these two types of spheres determined from the N_2

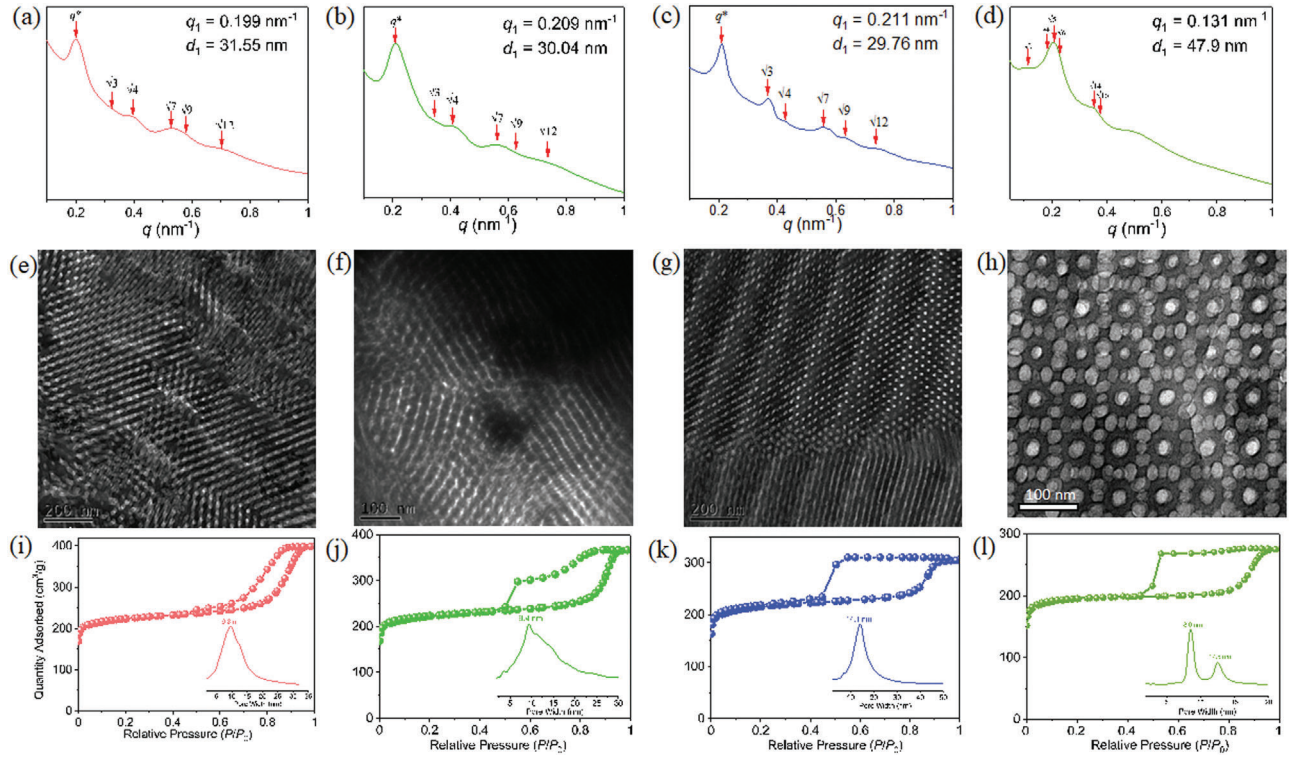

Figure 1. a–d) SAXS patterns, e–h) TEM images, and i–l) N_2 sorption/desorption isotherms of mesoporous phenolic/DDSQ hybrids derived from PDDSQ-30/EC mixtures: a,e,i) 50/50, b,f,j) 60/40, c,g,k) 70/30, and d,h,l) 80/20.

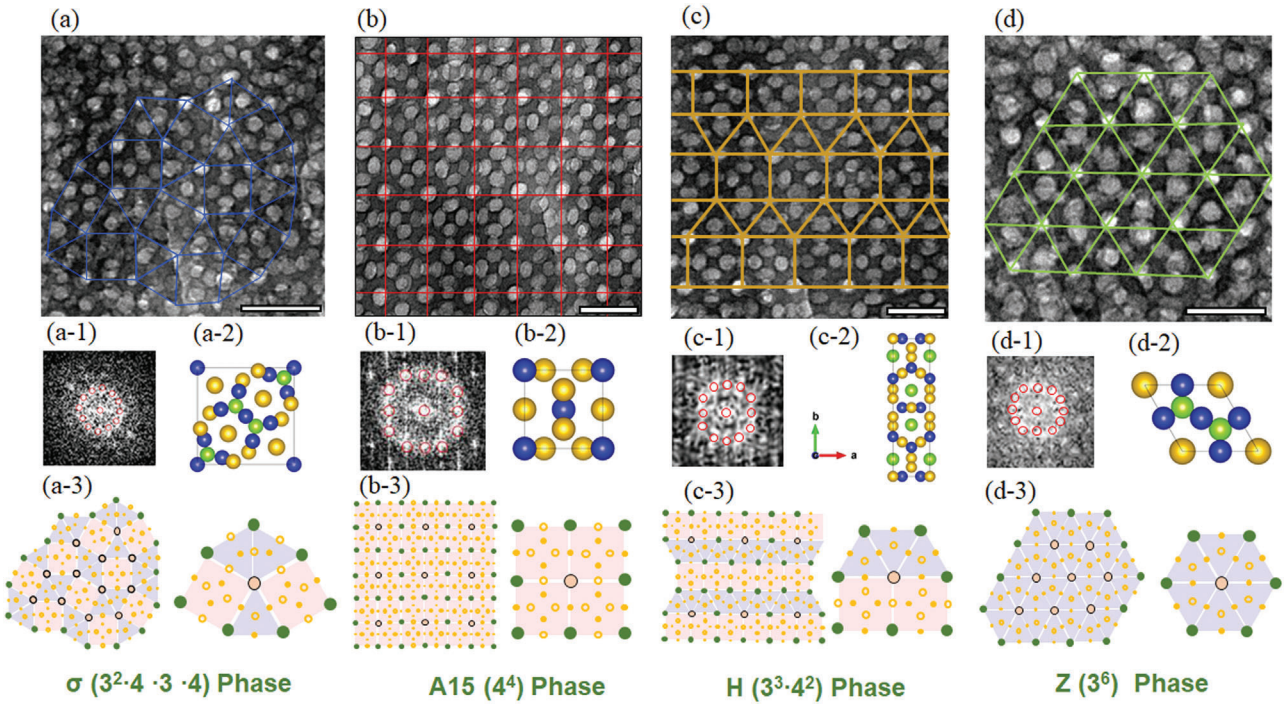

Figure 2. Mesoporous phenolic/DDSQ hybrids derived from PDDSQ-20/EC = 80/20 (a) TEM image, a-1) FFT diffraction pattern, a-2) FK σ phase, and a-3) $3^2.4.3.4$ tiling number of σ phase), PDDSQ-30/EC = 80/20 (b) TEM image, b-1) FFT diffraction pattern, b-2) FK A15 phase, and b-3) 4^4 tiling number of A15 phase), PDDSQ-50/EC = 80/20 (c) TEM image, c-1) FFT diffraction pattern, c-2) FK H phase, and c-3) $3^3.4^2$ tiling number of H phase), and PDDSQ-80/EC = 80/20 (d) TEM image, d-1) FFT diffraction pattern, d-2) FK Z phase, and d-3) 3^6 tiling number of Z phase).

sorption isotherms (1.45) was consistent with that from the TEM images, supporting the existence of two types of mesoporous spheres with different coordination environments in this mesoporous PDDSQ hybrid. We found that the mesoporous PDDSQ hybrid could also be obtained when using the linear symmetric PEO_{114}-*b*-PCL_{87} diblock copolymer (LAM phase) as the template. With hydrogen bonding occurring between the OH groups of the PDDSQ hybrid and the ether or C=O groups of the PEO-*b*-PCL diblock copolymer, this system exhibited "wet" brush behavior, transforming from LAM to HPC to A15 phases upon increasing the concentration of the PDDSQ hybrid in the PDDSQ/EC mixture, the result of an asymmetric composition of the PCL block segment—because the OH groups of PDDSQ preferred to interact with the PEO rather than PCL block segment (the inter-association equilibrium constant of phenolic/PEO [K_A = 286] is larger than that of phenolic/PCL blends [K_A = 116]).[21]

In previous studies,[14b,15d] we found that using this linear symmetric PEO_{114}-*b*-PCL_{87} diblock copolymer as the template for pure phenolic resin led only to typical DG, HPC, and BCC mesoporous structures, without the observation of any FK phases. Thus, in this present study, the presence of the DDSQ nanoparticles (NPs) in the phenolic matrix must have played an important role affecting the construction of the FK mesoporous structure. Because we could vary the amount of DDSQ in our PDDSQ hybrids (Table S1, Supporting Information), we prepared various PDDSQ-*x*/EC = 80/20 mixtures to investigate whether they would form mesoporous PDDSQ hybrids with different FK phases (**Figure 2**). To understand the complex nature of the FK phases, we began with the mesoporous PDDSQ hybrid

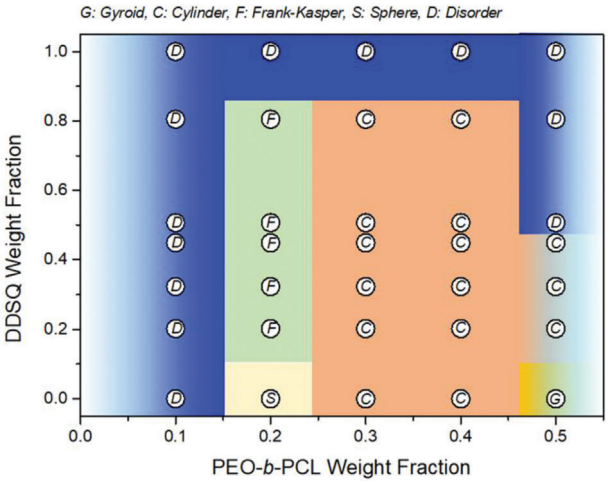

Figure 3. Phase diagram of mesoporous phenolic/DDSQ hybrids templated by EC diblock copolymer with FK phases found only in the PDDSQ-*x*/EC = 80/20 mixtures.

formed from the PDDSQ-20/EC = 80/20 mixture with the lowest DDSQ concentration in the PDDSQ hybrid. Figure 2a presents its corresponding TEM image along the [001] direction, with the typical $3^2.4.3.4$ tiling number (Figure 2a-**3**) of the FK σ phase determined from the fast Fourier transform (FFT) diffraction pattern (Figure 2a-1), indicating the tetragonal lattice of the FK σ phase (Figure 2a-2). The TEM image revealed a cube unit cell

with a calculated value of a of 63.46 ± 4.03 nm for the FK σ phase. Figure 2b provides the TEM image (Figure 1h)] of the mesoporous PDDSQ hybrid obtained from the PDDSQ-30/EC = 80/20 mixture along the [001] direction, with the typical 4^4 tiling number (Figure 2b-3) of the A15 phase (Figure 2b-2); its corresponding FFT diffraction pattern (Figure 2b-1) revealed the A15 phase along the [001] zone. Figure 2c displays the TEM image of the mesoporous PDDSQ hybrid prepared from the PDDSQ-50/EC = 80/20 mixture along the [001] direction, with the typical $3^3.4^2$ tiling number (Figure 2c-3) of the H phase (Figure 2c-2); the unit cell of the FK H phase had a value of a of 63.95 ± 2.35 and a value of b of 221.71± 3.24 nm, calculated from the TEM image. The corresponding FFT diffraction pattern (Figure 2c-1) revealed the H phase along the [001] zone. Further increasing the DDSQ concentration in PDDSQ to give the PDDSQ-80/EC = 80/20 mixture led to the formation of a mesoporous PDDSQ hybrid; its corresponding TEM image is provided in Figure 2d. Along the [001] direction, this sample displayed the typical 3^6 tiling number (Figure 2d-3) of the Z phase (Figure 2d-2); its unit cell had a value of a of 58.34 ± 6.04 nm. The corresponding FFT diffraction pattern (Figure 2d-1) revealed the Z phase along the [001] zone. Their corresponding SAXS patterns, the N_2 sorption isotherms and the pore size distribution are summarized in Figure S3, Supporting Information, Here, we need to emphasize the polydispersity (PDI = 1.3) problem of our PEO-*b*-PCL diblock copolymer as the template used in this study, which strongly affected the formation of FK phase and thus the highly ordered FK phase is difficult to observe in our study. As a result, the SAXS pattern is highly overlapped (Figure S3, Supporting Information) and quite difficult to identify in this work. However, two size distributions could be confirmed by N_2 sorptions (Figure S3e–h, Supporting Information) and TEM images (Figure 2) analyses, which provide the direct evidence of our FK phases in this study. Table S2, Supporting Information, summarizes the unit cell parameters and pore sizes for all of the FK phases of the mesoporous PDDSQ hybrids prepared from the various PDDSQ-x/EC = 80/20 mixtures based on N_2 sorptions and TEM images analyses.

Figures S4–S7, Supporting Information, display the characteristics of the mesoporous PDDSQ hybrids obtained from the other PDDSQ-x/EC mixtures (i.e., 90/10, 70/30, 60/40, 50/50). For example, Figure S4, Supporting Information, presents the SAXS patterns of the mesoporous PDDSQ hybrids prepared from the various PDDSQ-x/EC = 90/10 mixtures; these patterns all featured broad or disordered peaks, indicating that these porous hybrid materials possessed micelle or disordered porous structures. In contrast, the SAXS patterns of all of the mesoporous PDDSQ hybrids prepared from the various PDDSQ-x/EC = 70/30 and 60/40 mixtures (Figures S5a–f and S6a–f, Supporting Information) featured peak ratios of $1:\sqrt{3}:\sqrt{4}:\sqrt{7}:\sqrt{9}$—with some mixtures even exhibiting a peak at $\sqrt{12}$—indicating the long-range order of HPC mesostructures, as confirmed by their corresponding TEM images (Figures S5g–l and S6g–l, Supporting Information). Figure S7, Supporting Information, displays the SAXS patterns of the mesoporous PDDSQ hybrids obtained from the various PDDSQ-x/EC = 50/50 mixtures. The SAXS pattern of the mesoporous phenolic resin derived from the phenolic/EC = 50/50 mixture (Figure S7a, Supporting Information) featured a peak ratio of $\sqrt{6}:\sqrt{8}:\sqrt{10}:\sqrt{14}:\sqrt{22}:\sqrt{38}:\sqrt{50}$, implying the long-range order of a double-gyroid mesostructure, as through TEM imaging (Figure S7g, Supporting Information). After incorporation of DDSQ into the phenolic resin, SAXS analyses of the mesoporous PDDSQ hybrids derived from 50/50 mixtures of PDDSQ-20, PDDSQ-30, and PDDSQ-45 with EC revealed the long-range order of HPC mesostructures with a peak ratio of $1:\sqrt{3}:\sqrt{4}:\sqrt{7}:\sqrt{9}:\sqrt{12}$ (Figure S7b–d, Supporting Information), as confirmed by TEM (Figure S7h–j, Supporting Information). In addition, the mesoporous PDDSQ hybrids derived from the 50/50 mixtures of PDDSQ-50 and PDDSQ-80 with EC both displayed disordered porous structures, without any peak appearing in their SAXS patterns (Figure S7e,f, Supporting Information). Figure 3 provides the phase boundary diagram of the transition sequences and mesoporous structures, as determined from the SAXS and TEM data of these mesoporous PDDSQ hybrids templated by the EC diblock copolymer. Conventional mesophases—including DG, HPC, BCC, and Dis—were observed upon increasing the pure phenolic concentration. The FK phases were observed between the HPC and spheroidal micelle regions of the phase diagram, because of the compositional change, consistent with most recently predicted FK phase diagrams.[7] As a result, we conclude that the hydrogen bonding interactions in the PDDSQ hybrid with the EC diblock copolymer resulted in "wet" brush behavior that induced an asymmetric composition for the block segment, thereby forming FK phases through such a simple blending approach.

Because our mesoporous PDDSQ hybrids had high surface areas, high pore volumes, and tunable levels of Si and O heteroatoms derived from the DDSQ NPs, we suspected that these mesoporous hybrids might be suitable for supercapacitor applications after carbonization at 900 °C.[20,22] Accordingly, we selected the mesoporous carbon/DDSQ hybrids derived from the PDDSQ-x/EC = 80/20 mixtures, with various FK phases, for further study. **Figure 4**A displays the Raman spectra of our mesoporous carbon/DDSQ hybrids in the wavenumber range from 1200 to 1800 cm^{-1}. Two featured peaks were evident; one near 1592 cm^{-1}, due to the graphitic-carbonized structure (I_D), and the other near 1334 cm^{-1}, due to the disordered-carbonized structure.[20] The intensity ratio I_D/I_G of the mesoporous carbon/DDSQ hybrids could be used to determine the degree of graphitization. The values of I_D/I_G of the multiple heteroatom-doped mesoporous carbon/DDSQ hybrids obtained from the phenolic/EC, PDDQS-20/EC, PDDSQ-30/EC, PDDSQ-50/EC, and PDDSQ-80/EC = 80/20 samples were 0.92, 0.95, 0.83, 1.02, and 0.92, respectively, implying that the PDDSQ-50/EC = 80/20 hybrid possessed the most defected structure. Figure 4B provides the corresponding N_2 sorption isotherms of our mesoporous carbon/DDSQ hybrids. All of the mesoporous carbon/DDSQ hybrids provided typical type-IV curves, with sharp capillary condensations appearing at relative pressures ranging from 0.80 to 0.95 and H_2-like hysteresis loops, suggesting a common type of mesoporous structure with a cage-like morphology, consistent with the FK phase of the spheroidal micelle structures. Table S3, Supporting Information, summarizes the surface areas, total pore volumes, and pore sizes of our multiple heteroatom-doped mesoporous carbon/DDSQ hybrids, revealing that high surface areas, high pore volumes, and tunable Si and O heteroatom

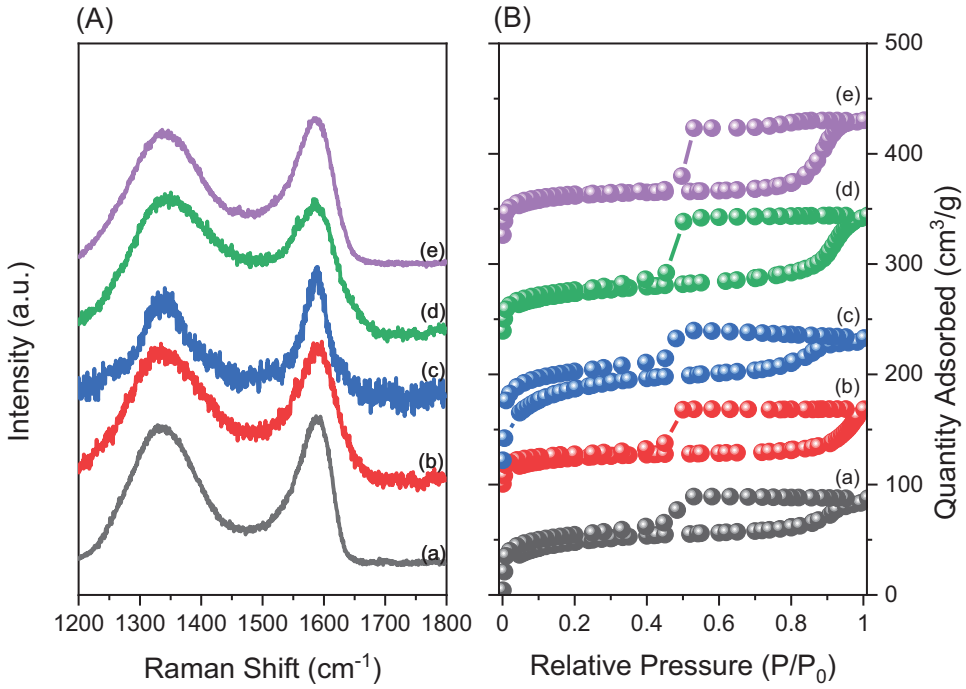

Figure 4. A) Raman spectra and B) N_2 sorption/desorption isotherms of mesoporous carbon/DDSQ hybrids derived from PDDSQ-*x*/EC = 80/20 mixtures: a) pure phenolic, b) PDDSQ-20, c) PDDSQ-30, d) PDDSQ-50, and e) PDDSQ-80.

contents were possible upon varying the DDSQ NP concentration in the PDDSQ hybrids.

We used cyclic voltammetry (CV) and galvanostatic charge–discharge (GCD) analyses to determine the electrochemical efficiencies of our mesoporous carbons (Figure S8a, Supporting Information) and carbon/DDSQ hybrids (Figure S8b–d, Supporting Information) in a three-electrode device in the presence of 1 M KOH as the basic aqueous electrolyte. We performed the CV measurements of our composites in the potential window from −1.00 to +0.35 V (versus Hg/HgO) at sweep rates ranging from 5 to 200 mV s^{-1} (Figure S9, Supporting Information). The mesoporous carbon/DDSQ hybrids provided CV curves having rectangle-like shapes featuring humps, implying that these mesoporous hybrids possessed supercapacitor behavior—a combination of a wide electric double-layer capacitor (EDLC) and a minor pseudocapacitor (PC).[22] The distinctive humps in the rectangle-like shapes arose from the O and few N atoms allowing reversible redox procedure in the mesoporous carbon/silica hybrids derived from the PDDQS-20/EC, PDDSQ-30/EC, and PDDSQ-50/EC = 80/20 hybrids.[22]

The GCD curves of the mesoporous carbon (**Figure 5**a) and carbon/DDSQ hybrids (Figure S8b–d, Supporting Information] were measured in 6 M KOH (as the electrolyte) at current densities from 0.5 to 20 A g^{-1}. The near-triangular shapes observed for the mesoporous carbon derived from the phenolic/EC mixture were characteristic of EDLC; in contrast, those observed for the mesoporous carbon/DDSQ hybrids were triangular with slight bends, suggesting the presence of both EDLC and PC. The discharging time of the mesoporous carbon/DDSQ hybrids increased upon increasing the concentration of DDSQ in the PDDSQ hybrid, implying that the existence of the DDSQ NPs in the mesoporous carbon enhanced the capacitance performance as a result of the presence of Si and O heteroatoms. We used Equation S1, Supporting Information, to calculate the specific capacitances of our mesoporous carbon/DDSQ hybrids from their GCD curves (Figure 5a). The specific capacitance of the mesoporous carbon derived from the phenolic/EC = 80/20 mixture was 100 F g^{-1}, while those of the mesoporous carbon/DDSQ hybrids derived from the PDDSQ-20/EC, PDDSQ-30/EC, and PDDSQ-50/EC = 80/20 mixtures were 195, 407, and 764 F g^{-1}, respectively, each measured at a current density of 0.5 A g^{-1}. The highest specific capacitance (764 F g^{-1}) was that of the mesoporous carbon/DDSQ hybrid prepared from the PDDSQ-50/EC = 80/20 mixture, presumably because of its high surface area, high pore volume, and high concentrations of Si and O heteroatoms, based on the XPS data (Table S4, Supporting Information), and its highly ordered FK phase at a similar pore size with other FK phases. These electroactive heteroatoms presumably made it easier for the electrolyte to access the electrode, while the DDSQ cage structure presumably provided many intercalated and fine channels for free passage of the electrolyte ions. The carbon material derived from PDDSQ-50 in the absence of the templating EC diblock copolymer provided a specific capacitance of only 258 F g^{-1}; thus, the high surface areas, controlled pore sizes, and well-defined mesopore structures of the mesoporous carbon/DDSQ hybrids all had strong effects on increasing the supercapacitor efficiency.[20] The diffusion length of the ion through the porous channel within the electrode was presumably shortened during the charge/discharge process, thereby enhancing the electrode capacitance efficiency. Furthermore, we examined the durabilities of our mesoporous carbon/DDSQ hybrids by cycling them at a current density of 10 A g^{-1} for up to

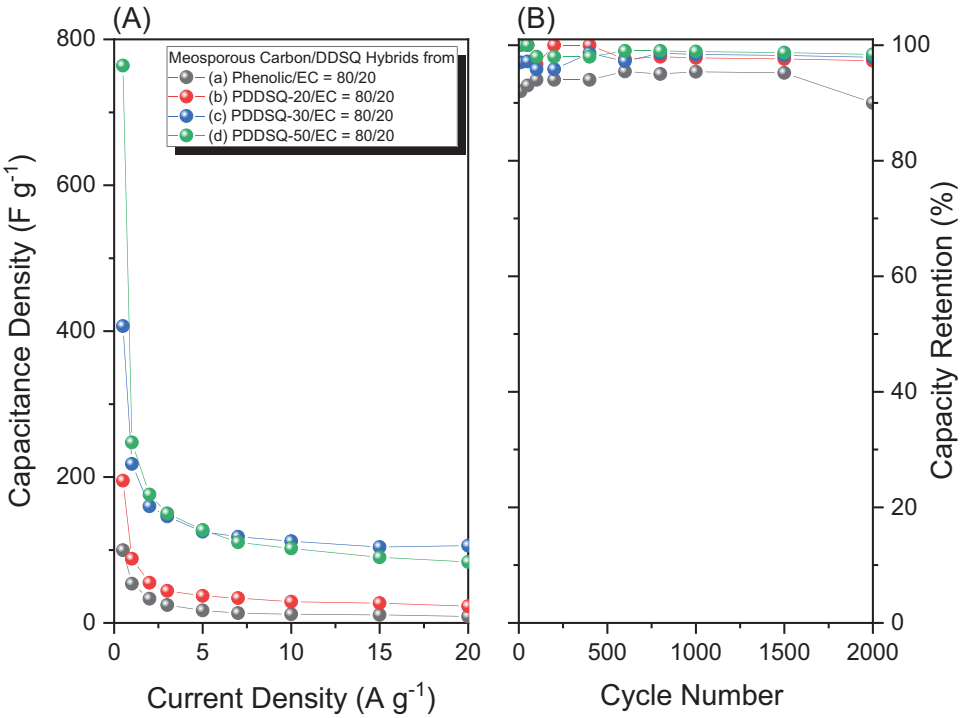

Figure 5. A) Specific capacitances (recorded at various scan rates) and B) cycling performance (recorded at a current density of 10 A g^{-1}) of mesoporous carbon/DDSQ hybrids derived from PDDSQ-*x*/EC = 80/20 mixtures: a) pure phenolic, b) PDDSQ-20, c) PDDSQ-30, and d) PDDSQ-50.

2000 cycles (Figure 5b). The mesoporous carbon/DDSQ hybrids derived from the phenolic/EC, PDDSQ-20/EC, PDDSQ-30/EC, and PDDSQ-50/EC = 80/20 mixtures displayed high stabilities, retaining 90.2%, 97.3%, 97.9%, and 98.4% of their initial capacitance, respectively. Furthermore, the SEM image (Figure S10, Supporting Information) after the cycling about the morphology of mesoporous carbon/DDSQ hybrid from PDDSQ-50/EC = 80/20, the electrode shows still smooth, and the C, Si, N, and O atoms still remained, indicating the morphology did change after the 2000 cycles. Table S5, Supporting Information, summarizes that other mesoporous carbons, silica and carbon/silica composites have not displayed such strong performance, of which the electrochemical results of our mesoporous hybrids are considered much higher than other reported ones.[15d,23]

3. Conclusions

We have developed a new strategy for the synthesis of mesoporous FK phases: by varying the DDSQ concentration in PDDSQ hybrids templated by an unusual symmetry linear PEO-*b*-PCL diblock copolymer. We obtained various mesoporous FK phases—namely, σ, A15, H, and Z phases—upon increasing the DDSQ content in PDDSQ/EC = 80/20 hybrids; SAXS and TEM analyses allowed us to determine the phase boundary diagram of the transition sequences and the nature of the mesoporous structures. Furthermore, our mesoporous carbon/DDSQ hybrids possessed high surface areas, high pore volumes, and high contents of Si and O heteroatoms, encouraging us to test them as electrode materials for energy storage applications. Our optimized sample provided a significant specific capacitance of 764 F g^{-1} at a current density of 0.5 A g^{-1}, with a stability of 98.4% after 2000 cycles at a current density of 10 A g^{-1}. Thus, this study provides a direct and facile approach for the preparation of mesoporous FK phases—without the need for complicated syntheses of asymmetric complex tetrablock copolymers, architecturally giant molecules, or surfactants—as well as an effective method toward materials for high-performance energy storage. This material is also suitable for lithium batteries for the surface coating between Si and carbon materials, as the anode electrode that still worked in our group.

Supporting Information

Supporting Information is available from the Wiley Online Library or from the author.

Acknowledgements

This study was supported financially by the Ministry of Science and Technology, Taiwan, under contracts MOST 108-2218-E-110-013-MY3 and 109-2221-E-110-067-MY3.

Conflict of Interest

The authors declare no conflict of interest.

Data Availability Statement

Research data are not shared.

Keywords

block copolymers, Frank-Kasper phase, hybrids, mesoporous materials, supercapacitors

Received: May 12, 2021
Revised: June 18, 2021
Published online: July 3, 2021

[1] a) K. Kim, M. W. Schulze, A. Arora, R. M. Lewis, M. A. Hillmyer, K. D. Dorfman, F. S. Bates, *Science* **2017**, *356*, 520; b) Z. Su, J. Huang, W. Shan, X. Y. Yan, R. Zhang, T. Liu, Y. Liu, Q. Y. Guo, F. Bian, X. Miao, M. Huang, S. Z. D. Cheng, *CCS Chem.* **2021**, *3*, 1434; c) K. K. Lachmayr, C. M. Wentz, L. R. Sita, *Angew. Chem., Int. Ed.* **2020**, *59*, 1521; d) A. Jayaraman, D. Y. Zhang, B. L. Dewing, M. K. Mahanthappa, *ACS Cent. Sci.* **2019**, *5*, 619.

[2] a) S. Lee, M. J. Bluemle, F. S. Bates, *Science* **2010**, *330*, 349; b) B.-K. Cho, *Science* **2004**, *305*, 1598; c) H.-J. Sun, S. Zhang, V. Percec, *Chem. Soc. Rev.* **2015**, *44*, 3900; d) G. Ungar, X. Zeng, *Soft Matter* **2005**, *1*, 95; e) X. H. Cheng, S. Diele, C. Tschierske, *Angew. Chem., Int. Ed.* **2000**, *39*, 592; f) M. Huang, K. Yue, J. Wang, C.-H. Hsu, L. Wang, S. Z. D. Cheng, *Sci. China Chem.* **2018**, *61*, 33; g) S. Lee, C. Leighton, F. S. Bates, *Proc. Natl. Acad. Sci. U. S. A.* **2014**, *111*, 17723; h) K. K. Lachmayr, L. R. Sita, *Angew. Chem., Int. Ed.* **2020**, *59*, 3563.

[3] a) A. B. Chang, F. S. Bates, *ACS Nano* **2020**, *14*, 11463; b) M. Watanabe, Y. Asai, J. Suzuki, A. Takano, Y. Matsushita, *Macromolecules* **2020**, *53*, 10217.

[4] a) H.-A. Klok, S. Lecommandoux, *Adv. Mater.* **2001**, *13*, 1217; b) J. K. Kim, S. Y. Yang, Y. Lee, Y. Kim, *Prog. Polym. Sci.* **2010**, *35*, 1325.

[5] G. K. Cheong, F. S. Bates, K. D. Dorfman, *Proc. Natl. Acad. Sci. U. S. A.* **2020**, *117*, 16764.

[6] a) M. W. Bates, S. M. Barbon, A. E. Levi, R. M. Lewis, H. K. Beech, K. M. Vonk, C. Zhang, G. H. Fredrickson, C. J. Hawker, C. M. Bates, *ACS Macro Lett.* **2020**, *9*, 396; b) N. Xie, W. Li, F. Qiu, A. N.-C. Shi, *ACS Macro Lett.* **2014**, *3*, 906; c) M. Zhao, W. Li, *Macromolecules* **2019**, *52*, 1832.

[7] M. W. Bates, J. Lequieu, S. M. Barbon, R. M. Lewis, K. T. Delaney, A. Anastasaki, C. J. Hawker, G. H. Fredrickson, C. M. Bates, *Proc. Natl. Acad. Sci. U. S. A.* **2019**, *116*, 13194.

[8] a) S. Liu, N. C. Billingham, S. P. Armes, *Angew. Chem., Int. Ed.* **2001**, *113*, 2390; b) Y. Yagci, M. Atilla Tasdelen, *Prog. Polym. Sci.* **2006**, *31*, 1133; c) D. T. Gentekos, R. J. Sifri, B. P. Fors, *Nat. Rev. Mater.* **2019**, *4*, 761.

[9] a) A. J. Mueller, A. P. Lindsay, A. Jayaraman, T. P. Lodge, M. K. Mahanthappa, F. S. Bates, *ACS Macro Lett.* **2020**, *9*, 576; b) Z. Su, M. Huang, S. Z. D. Cheng, *Proc. Natl. Acad. Sci. U. S. A.* **2020**, *117*, 19618.

[10] a) K. Dobrosielska, S. Wakao, A. Takano, Y. Matsushita, *Macromolecules* **2008**, *41*, 7695; b) K. Dobrosielska, S. Wakao, J. Suzuki, K. Noda, A. Takano, Y. Matsushita, *Macromolecules* **2009**, *42*, 7098; c) A. Dehghan, A. N.-C. Shi, *Macromolecules* **2013**, *46*, 5796; d) N. Hameed, J. Liu, Q. Guo, *Macromolecules* **2008**, *41*, 7596; e) W.-C. Chen, S.-W. Kuo, C.-H. Lu, U.-S. Jeng, F.-C. Chang, *Macromolecules* **2009**, *42*, 3580; f) N. Hameed, N. V. Salim, Q. Guo, *J. Chem. Phys.* **2009**, *131*, 214905; g) C.-T. Tsou, S.-W. Kuo, *Macromolecules* **2019**, *52*, 8374; h) T.-C. Tseng, S.-W. Kuo, *Macromolecules* **2018**, *51*, 6451; i) S.-W. Kuo, *Polym. Int.* **2021**, https://doi.org/10.1002/pi.6264; j) M. G. Mohamed, E. C. Atayde, B. M. Matsagar, J. Na, Y. Yamauchi, K. C.-W. Wu, S.-W. Kuo, *J. Taiwan Inst. Chem. Eng.* **2020**, *112*, 180.

[11] a) S.-C. Chen, S.-W. Kuo, U.-S. Jeng, C.-J. Su, F.-C. Chang, *Macromolecules* **2010**, *43*, 1083; b) S.-C. Tsai, Y.-C. Lin, E.n-L.i Lin, Y.-W. Chiang, S.-W. Kuo, *Polym. Chem.* **2016**, *7*, 2395.

[12] a) R. Ryoo, S. H. Joo, M. Kruk, M. Jaroniec, *Adv. Mater.* **2001**, *13*, 677; b) M. Vallet-Regí, F. Balas, D. Arcos, *Angew. Chem., Int. Ed.* **2007**, *46*, 7548; c) J. Tang, J. Liu, C. Li, Y. Li, M. O. Tade, S. Dai, Y. Yamauchi, *Angew. Chem., Int. Ed.* **2015**, *54*, 588; d) Y. Wan, Zhao, *Chem. Rev.* **2007**, *107*, 2821; e) J. Liu, L. Xie, Z. Wang, S. Mao, Y. Gong, Y. Wang, *Chem. Commun.* **2005**, *56*, 229; f) X. Xu, H. Tan, Z. Wang, C. Wang, L. Pan, Y. V. Kaneti, T. Yang, Y. Yamauchi, *Environ. Sci.: Nano* **2019**, *6*, 981; g) P. Wang, G. Zhang, W. Chen, Q. Chen, H. Jiao, L. Liu, X. Wang, X. Deng, *ACS Omega* **2020**, *5*, 23460; h) L. Wang, J. Wu, H. Ma, G. Han, D. Yang, Y.u Chen, J. Zhou, *Energy Fuels* **2021**, *35*, 8303; i) S. Zhang, W. Xia, Q. Yang, Y. Valentino Kaneti, X. Xu, S. M. Alshehri, T. Ahamad, M. S. A. Hossain, J. Na, J. Tang, Y. Yamauchi, *Chem. Eng. J.* **2020**, *396*, 125154.

[13] a) Y. Sun, K. Ma, T. Kao, K. A. Spoth, H. Sai, D. Zhang, L. F. Kourkoutis, V. Elser, U. Wiesner, *Nat. Commun.* **2017**, *8*, 252; b) C. Xiao, N. Fujita, K. Miyasaka, Y. Sakamoto, O. Terasaki, *Nature* **2012**, *487*, 349.

[14] a) Y. Deng, T. Yu, Y. Wan, Y. Shi, Y. Meng, D. Gu, L. Zhang, Y. Huang, C. Liu, X. Wu, D. Zhao, *J. Am. Chem. Soc.* **2007**, *129*, 1690; b) J.-G. Li, Y.-D. Lin, S.-W. Kuo, *Macromolecules* **2011**, *44*, 9295; c) J. Wei, Q. Yue, Z. Sun, Y. Deng, D. Zhao, *Angew. Chem., Int. Ed.* **2012**, *124*, 6253.

[15] a) J.-G. Li, C.-Y.u Chung, S.-W. Kuo, *J. Mater. Chem.* **2012**, *22*, 18583; b) C.-C. Liu, W.-C. Chu, J.-G. Li, S.-W. Kuo, *Macromolecules* **2014**, *47*, 6389; c) J.-G. Li, R.-B. Lin, S.-W. Kuo, *Macromol. Rapid Commun.* **2012**, *33*, 678; d) J.-G. Li, Y.a-F. Ho, M. M. M. Ahmed, H.-C. Liang, S.-W. Kuo, *Chem. - Eur. J.* **2019**, *25*, 10456; e) A. F. M. El-Mahdy, T. C. Yu, M. G. Mohamed, S.-W. Kuo, *Macromolecules* **2021**, *54*, 1030; f) A. F. M. El-Mahdy, T.-E.n Liu, S.-W. Kuo, *J. Hazard. Mater.* **2020**, *391*, 122163.

[16] M. Huang, C.-H. Hsu, J. Wang, S. Mei, X. Dong, Y. Li, M. Li, H. Liu, W. Zhang, T. Aida, W.-B. Zhang, K. Yue, S. Z. D. Cheng, *Science* **2015**, *348*, 424.

[17] a) K. Yue, M. Huang, R. L. Marson, J. He, J. Huang, Z. Zhou, J. Wang, C. Liu, X. Yan, K. Wu, Z. Guo, H. Liu, W. Zhang, P. Ni, C. Wesdemiotis, W.-B. Zhang, S. C. Glotzer, S. Z. D. Cheng, *Proc. Natl. Acad. Sci. U. S. A.* **2016**, *113*, 14195; b) Z. Su, C.-H. Hsu, Z. Gong, X. Feng, J. Huang, R. Zhang, Y.u Wang, J. Mao, C. Wesdemiotis, T. Li, S. Seifert, W. Zhang, T. Aida, M. Huang, S. Z. D. Cheng, *Nat. Chem.* **2019**, *11*, 899; c) Z. Su, R. Zhang, X.-Y. Yan, Q.-Y. Guo, J. Huang, W. Shan, Y. Liu, T. Liu, M. Huang, S. Z. D. Cheng, *Prog. Polym. Sci.* **2020**, *103*, 101230.

[18] S.-W. Kuo, F.-C. Chang, *Prog. Polym. Sci.* **2011**, *36*, 1649.

[19] H.-C. Lin, S.-W. Kuo, C.-F. Huang, F.-C. Chang, *Macromol. Rapid Commun.* **2006**, *27*, 537.

[20] W.-C. Chen, Y.-T. Liu, S.-W. Kuo, *Polymers* **2020**, *12*, 2151.

[21] S. W. Kuo, *Hydrogen Bonding in Polymeric Materials*, John Wiley & Sons, Hoboken, NJ **2018**.

[22] a) A. F. M. El-Mahdy, T. C. Yu, S.-W. Kuo, *Chem. Eng. J.* **2021**, *414*, 128796; b) H. R. Abuzeid, A. F. M. El-Mahdy, S.-W. Kuo, *Giant* **2021**, *6*, 100054; c) M. M. Samy, M. G. Mohamed, S.-W. Kuo, *Compos. Sci. Tech.* **2020**, *199*, 108360; d) A. F. M. El-Mahdy, M. B. Zakaria, H.-X. Wang, T. Chen, Y. Yamauchi, S.-W. Kuo, *J. Mater. Chem. A* **2020**, *8*, 25148.

[23] a) M. G. Mohamed, W.-S. Hung, A. F. M. El-Mahdy, M. M. M. Ahmed, L. Dai, T. Chen, S.-W. Kuo, *Polymers* **2020**, *12*, 1193; b) J. Cao, C. J. Jafta, J. Gong, Q. Ran, X. Lin, R. Félix, R. G. Wilks, M. Bär, J. Yuan, M. Ballauff, Y. Lu, *ACS Appl. Mater. Interfaces* **2016**, *8*, 29628; c) J. Da, Y. Zhang, H. Wu, S. Hou, A. Chen, *Carbon* **2020**, *156*, 523; d) K. Liang, C. Ma, L. Liu, Y. Yu, H. Lv, Y. Zhang, A. Chen, *J. Alloys Compd.* **2019**, *805*, 859; e) M. M. Samy, M. G. Mohamed, S.-W. Kuo, *Compos. Sci. Technol.* **2020**, *199*, 108360.

